Regulation of calreticulin–major histocompatibility complex (MHC) class I interactions by ATP

Sanjeeva Joseph Wijeyesakere[a], Jessica K. Gagnon[b], Karunesh Arora[b], Charles L. Brooks III[b], and Malini Raghavan[a,1]

[a]Department of Microbiology and Immunology, University of Michigan Medical School, Ann Arbor, MI 48109; and [b]Department of Chemistry, University of Michigan, Ann Arbor, MI 48109

Edited by Peter Cresswell, Yale University School of Medicine, New Haven, CT, and approved September 1, 2015 (received for review May 26, 2015)

The MHC class I peptide loading complex (PLC) facilitates the assembly of MHC class I molecules with peptides, but factors that regulate the stability and dynamics of the assembly complex are largely uncharacterized. Based on initial findings that ATP, in addition to MHC class I-specific peptide, is able to induce MHC class I dissociation from the PLC, we investigated the interaction of ATP with the chaperone calreticulin, an endoplasmic reticulum (ER) luminal, calcium-binding component of the PLC that is known to bind ATP. We combined computational and experimental measurements to identify residues within the globular domain of calreticulin, in proximity to the high-affinity calcium-binding site, that are important for high-affinity ATP binding and for ATPase activity. High-affinity calcium binding by calreticulin is required for optimal nucleotide binding, but both ATP and ADP destabilize enthalpy-driven high-affinity calcium binding to calreticulin. ATP also selectively destabilizes the interaction of calreticulin with cellular substrates, including MHC class I molecules. Calreticulin mutants that affect ATP or high-affinity calcium binding display prolonged associations with monoglucosylated forms of cellular MHC class I, delaying MHC class I dissociation from the PLC and their transit through the secretory pathway. These studies reveal central roles for ATP and calcium binding as regulators of calreticulin–substrate interactions and as key determinants of PLC dynamics.

calreticulin | ATP | ATPase | MHC class | monoglucosylated glycans

MHC class I molecules are ligands for the antigen receptors of $CD8^+$ T cells and natural killer cells. The assembly and folding of MHC class I molecules with antigenic peptides take place within the endoplasmic reticulum (ER) and are facilitated by a multiprotein complex called the peptide loading complex (PLC) (reviewed in 1, 2). Structurally, the PLC involves the association of MHC class I heterodimers with the transporter associated with antigen processing (TAP), an interaction bridged, via several protein–protein interactions, within the ER lumen. Tapasin interacts with TAP via its transmembrane domain and with MHC class I via its ER luminal domains. MHC class I molecules also interact with the glycan-binding chaperone calreticulin through a conserved glycan on the α2-domain of the MHC class I heavy chain (3, 4). The thiol oxidoreductase ERp57, which functions as a cellular cochaperone for calreticulin (CRT), forms a disulfide-linked heterodimer with tapasin (reviewed in 1). In this manner, by bridging interactions with MHC class I and tapasin, respectively, calreticulin and ERp57 stabilize the binding of MHC class I molecules to tapasin–TAP complexes (reviewed in 1, 2). Cellular deficiencies in calreticulin and ERp57 destabilize MHC class I interactions with other components of the PLC (5–8). Furthermore, peptide binding to MHC class I has been shown to destabilize MHC class I–tapasin interactions (9, 10), but how other cellular factors influence PLC stability is largely uncharacterized.

In this investigation, we show that ATP destabilizes MHC class I interactions with PLC components. ATP is a known regulator of substrate interactions with several cellular chaperones. Calreticulin, like several other chaperones, is known to interact with ATP (8, 11, 12). However, the location of the calreticulin-ATP–binding site is unknown, as is the influence of ATP on calreticulin binding to cellular substrates, including MHC class I. In this study, using computational methods validated by experimental approaches, we identify residues within the globular domain of calreticulin that are important for ATP binding and ATPase activity. Based on further investigations into the functional effects of calreticulin mutants with deficiencies in ATP interactions, we elucidate a key role for ATP in the regulation of PLC dynamics and the interaction of calreticulin with other cellular proteins.

Results

ATP Destabilizes the PLC, Promoting MHC Class I Release. Calreticulin-deficient mouse embryonic fibroblasts (MEFs) reconstituted with wild type (WT) murine calreticulin [mCRT(WT)] were pulsed with [^{35}S]-methionine, and the ability of ATP or peptide to stimulate dissociation of MHC class I from immunoisolated TAP complexes was measured. Relative to the buffer control, the addition of 4 mM ATP [an ATP concentration close to physiological levels (13)] promoted the elution of MHC class I from TAP (Fig. 1*A*, lane 3). Likewise, consistent with the known ability of MHC class I-specific peptides to regulate PLC stability (reviewed in 1), MHC class I release was induced via the addition of an H2-K^b–specific peptide (SIINFEKL) (Fig. 1*A*, lane 4). Taken together, these findings suggested that ATP, like MHC class I-specific peptides, plays a role in destabilizing PLC interactions.

ATP Interacts at a Site Within the Globular Domain of Calreticulin. Structurally, calreticulin contains three domains (Fig. 1*B*): (*i*) a globular domain comprising a lectin fold that contains its glycan and polypeptide-substrate–binding sites (14–17) and a single high-affinity calcium-binding site (18, 19), (*ii*) an arm-like Pro-rich domain (termed the P-domain) that binds the cochaperones ERp57 (20, 21) and cyclophilin-B (22) and mediates interactions of calreticulin with nonglycosylated proteins (17), and (*iii*) an acidic C-terminal region

Significance

Calreticulin mutants that disrupt ATP binding are shown to prolong cellular MHC class I interactions with calreticulin and with the transporter associated with antigen processing (TAP). To our knowledge, no previous studies have implicated a role for endoplasmic reticulum (ER) luminal ATP as a determinant of MHC class I assembly complex dynamics. These studies also reveal a role for the ATP–calreticulin interaction in broadly regulating the binding of calreticulin to cellular substrates. Because a large number of cell surface and secreted glycoproteins are calreticulin/calnexin substrates, these studies have broad significance toward understanding the cellular mechanisms of protein quality control.

Author contributions: S.J.W., J.K.G., K.A., C.L.B., and M.R. designed research; S.J.W., J.K.G., and K.A. performed research; S.J.W., J.K.G., K.A., and M.R. analyzed data; and S.J.W., J.K.G., K.A., and M.R. wrote the paper.

The authors declare no conflict of interest.

This article is a PNAS Direct Submission.

[1]To whom correspondence should be addressed. Email: malinir@umich.edu.

This article contains supporting information online at www.pnas.org/lookup/suppl/doi:10.1073/pnas.1510132112/-/DCSupplemental.

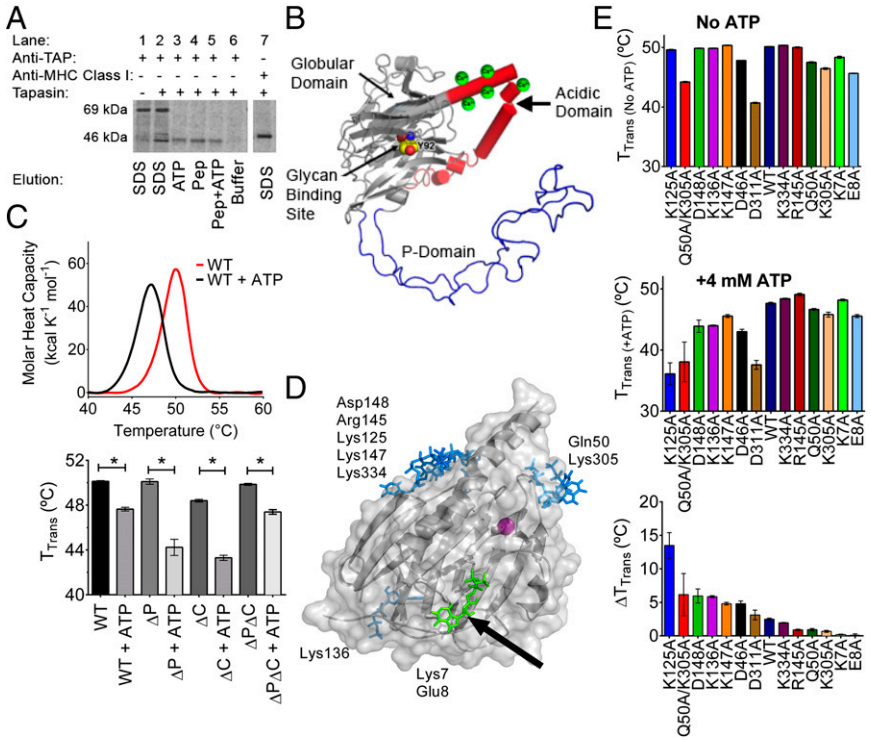

Fig. 1. ATP induces dissociation of MHC class I from the PLC (*A*) and interacts with the globular domain of calreticulin (*B–E*). (*A*) Gel panel shows a representative anti-TAP IP of lysates from [^{35}S]-methionine–labeled CRT$^{-/-}$ MEFs expressing mCRT(WT). The resulting IPs were eluted with SDS (lanes 1 and 2), ATP (lane 3), the SIINFEKL peptide (Pep; lane 4), the SIINFEKL peptide together with ATP (lane 5), or buffer alone (lane 6). Lane 1 is a negative control of an anti-TAP IP using lysates from tapasin-deficient cells that are impaired for MHC class I-TAP binding. Lane 7 shows a direct MHC class I (Y3) IP from CRT$^{-/-}$ MEFs to mark the migration position of MHC class I. Data are representative of three independent experiments. (*B*) Model for calreticulin showing its globular, P-terminal, and C-terminal domains. The globular domain structure (gray) is based on PDB ID code 3O0V (15), the P-domain structure (blue) is based on PDB ID code 1HHN (45), and the P-domain orientation is modeled based on PDB ID code 3RG0 (16). The acidic domain [modeled de novo using I-TASSER (46)] is indicated in red, with multiple low-affinity calcium-binding sites (shown as green spheres). The glycan-binding residue Tyr92 on the concave surface of the globular domain is indicated (atoms are represented as spheres with carbon colored yellow, oxygen colored red, and nitrogen colored blue). (*C*, *Upper*) Representative DSC thermograms showing the thermostability of calreticulin in the absence or presence of 4 mM ATP. (*C*, *Lower*) Quantification of thermostability change (T_{Trans}) values for calreticulin constructs containing or lacking the P-domain, acidic domain, or both [mCRT(ΔP), mCRT(ΔC), and mCRT(ΔPΔC)] in the presence or absence of 4 mM ATP. Data show the mean ± SEM from two to three [mCRT(ΔC), mCRT(ΔP), and mCRT(ΔPΔC)] or 27 [mCRT(WT)] independent experiments. Statistically significant differences in the mean T_{Trans} values (assessed via a one-way ANOVA, followed by a Tukey's post hoc test) are denoted (*). (*D*) Global docking of ATP to the globular domain of mCRT [PDB ID code 3O0V (15)]. Key nucleotide-interacting residues from each cluster are noted. An arrow denotes the cluster of poses in close proximity to Lys7 (green). (*E*) Interaction of calreticulin point mutants with ATP. Plots show the mean T_{Trans} values (±SEM) in the absence of ATP (*Upper*) and in the presence of 4 mM ATP (*Middle*), and the ATP-induced change in the T_{Trans} values (ΔT_{Trans}) (*Lower*). Data represent the mean T_{Trans} ± SEM from two to four (mutants) or 27 [mCRT(WT)] independent experiments.

containing several low-affinity calcium-binding sites (18, 19) that function in ER calcium homeostasis (23).

Using differential scanning calorimetry (DSC), we found that 4 mM ATP decreased the thermostability of mCRT(WT) (Fig. 1*C*), consistent with previous findings using a different thermostability assay (8). Similar reductions in thermostability are seen for calreticulin constructs lacking the P-domain [mCRT(ΔP)], the acidic C-terminal domain [mCRT(ΔC)], or both the P-domain and acidic C-terminal domain [mCRT(ΔPΔC)] (Fig. 1*C*), indicating that a nucleotide-binding site of calreticulin is localized within its globular domain.

We used structure-based docking to predict putative nucleotide-binding sites further. ATP was docked to the crystal structure of the globular domain of calreticulin [Protein Data Bank (PDB) ID code 3O0V] (15). A consensus docking approach was used, with results from Autodock Vina compared with results from CDOCKER [CHARMM simulation package (24–26)]. The Autodock Vina results were rescored with CHARMM in implicit solvent to compare results from the two docking software packages with the same scoring approach (27, 28). There were four clusters of ATP conformations that scored favorably with both docking methodologies, as shown in Fig. 1*D*.

We mutated residues around the predicted binding sites and tested the mutants for ATP binding using the DSC assay. Following the addition of ATP, several of the tested mutants showed thermostability reductions comparable to those thermostability reductions seen with mCRT(WT). Mutants with reduced ATP-induced thermostability changes (ΔT_{Trans}) were mCRT(K7A), mCRT(E8A), mCRT(Q50A), mCRT(K305A), mCRT(K334A), and mCRT(R145A) (Fig. 1*E*). The smallest ATP-induced thermostability reductions were noted for mCRT(K7A) and mCRT(E8A).

Nucleotides can quench the intrinsic Trp fluorescence of calreticulin (12). By measuring the quenching of the Trp fluorescence of calreticulin in the presence of varying concentrations of ATP and ADP, relative binding affinities of the different mutants could be quantitatively compared. mCRT(WT) interacts with ATP and ADP with steady-state affinities of 0.65 ± 0.09 mM and 1.02 ± 0.21 mM, respectively (Fig. 2*A* and Table 1). These affinities are similar to the nucleotide affinity reported for other chaperones like heat shock protein 90 (HSP90) (29). Defective ATP binding was seen with mCRT(K7A) (K_d = 6.33 ± 0.70 mM) and mCRT(E8A) (K_d = 5.49 ± 1.45 mM) (Fig. 2*A* and Table 1). However, mCRT(K334A), mCRT(R145A), and mCRT(K305A) bound ATP with affinities similar to those affinities observed for mCRT(WT) (Fig. 2*A* and Table 1). The affinity of mCRT(Q50A)

toward ATP (1.18 ± 0.25 mM) was 1.5-fold lower than the affinity observed for mCRT(WT), but greater than fivefold higher than the affinity seen with mCRT(K7A) and mCRT(E8A) (Fig. 2*A* and Table 1). Also, the mCRT(Q50A/K305A) construct showed a greater ATP-induced thermostability change relative to mCRT(WT), mCRT(Q50A), and mCRT(K305A) (Fig. 1*E*). Gln50 and Lys305 are located on flexible loops rather than structured pockets (Fig. 1*D*). Thus, these findings pointed to the involvement of Lys7 and Glu8, rather than Gln50 and Lys305, in ATP binding.

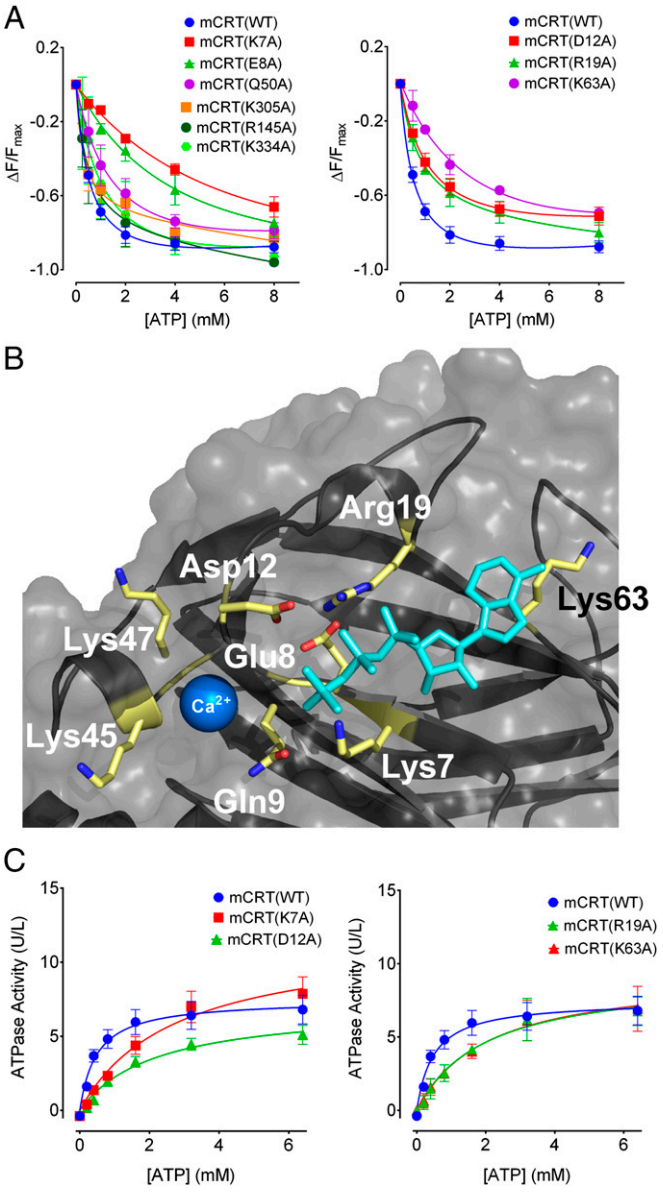

Fig. 2. Residues in proximity to the high-affinity calcium-binding site affect ATP binding and hydrolysis. (*A*) Plots showing the dose-dependent quenching of the intrinsic Trp fluorescence of the indicated calreticulin constructs in the presence of varying concentrations of ATP. Derived binding constants and numbers of experimental replicates are shown in Table 1. (*B*) Time-averaged structure of the highest scoring pose of ATP docked within the putative nucleotide-binding site defined by Lys7. Lys7, Glu8, Asp12, Arg19, and Lys63 are shown as sticks. The Ca^{2+} ion is shown as a blue sphere within the previously defined high-affinity calcium-binding site [from PDB ID code 3O0V (15)]. (*C*) Michaelis–Menten kinetic plots depicting ATP hydrolysis as a function of ATP concentration. Data show mean ± SEM, with Michaelis constants and data replicates shown in Table 1.

Lys7 and Glu8 could indirectly affect ATP binding or directly comprise an ATP-binding site, as suggested by the results of the docking studies (Fig. 1*D*). To assess the latter possibility further, we docked ATP to an area centered on the Cα atom of Lys7, followed by molecular dynamics (MD) simulations of the ATP configuration with the lowest predicted binding energy (30–32). The simulations showed that Lys7 interacts with the α-phosphate of ATP (Fig. 2*B*). Additionally, when Lys7 was mutated to an Ala in silico, MD simulations of the mCRT(K7A)–ATP complex showed the nucleotide dissociating from calreticulin within the first 10 ns of the simulation, a time point at which the nucleotide was still bound to mCRT(WT) (Movies S1 and S2), suggesting a direct role for Lys7. MD simulations also showed contact between Lys63 and the nucleotide base of ATP, and that Glu8 interacts with the β-phosphate of ATP (Fig. 2*B*). Hydrogen bonding between Arg19 and Asp12 is predicted to stabilize these residues in an orientation favorable for interaction with the γ-phosphate of ATP, implicating Asp12 and Arg19 as putative catalytic residues (Fig. 2*B*). MD simulations of the modeled ATP–calreticulin complex in the presence of 0.15 M NaCl showed Na^+ ions from the bulk solvent interacting with ATP and orienting the γ-phosphate of ATP toward Asp12 and Arg19 (Fig. S1*A*). Similar results were seen for MD simulations in the presence of divalent Mg^{2+} ions. Multiple Mg^{2+} ions from bulk solvent interacted with the γ-phosphate of ATP (Fig. S1*B*). Although calreticulin lacks the common nucleotide-binding Walker-A and Walker-B sequences, Asp12 is contained within a DXD motif that is suggested to be an alternative to a Walker-B motif in mediating interactions with divalent cations during ATP hydrolysis (33).

Guided by these findings, we also tested calreticulin constructs containing Ala point mutations at Asp12, Arg19, and Lys63 for their abilities to bind ATP via fluorescence quenching. mCRT(K63A) displayed a decreased affinity for ATP (K_d = 2.69 ± 0.58 mM) relative to mCRT(WT) (Fig. 2*A* and Table 1). On the other hand, mCRT(D12A) and mCRT(R19A) bound ATP with affinities that were similar to those affinities observed for mCRT(WT) (Fig. 2 *A* and *B* and Table 1). For all constructs, similar affinities were derived for calreticulin-ADP binding as for ATP binding (Table 1).

Calreticulin-Derived Divalent Cation-Dependent ATPase Activity. A weak ATPase activity has previously been reported for calreticulin (12). We found that mCRT(WT) hydrolyzes ATP with a Michaelis–Menten constant (K_m) of 0.47 ± 0.03 mM (Fig. 2*C* and Table 1) and a corresponding turnover number (k_{cat}) of 34.02 ± 3.12 min^{-1}. The calculated K_m for the ATPase activity of mCRT(WT) is similar to its affinity for ATP (Table 1). The turnover number for the ATPase activity of mCRT(WT) is similar to the turnover number for chaperones like HSP90 (34). The interaction of calreticulin with magnesium is predicted to drive hydrolysis of ATP (Fig. S1*B*), whereas calcium binding may contribute a structural role based on previous studies (19) and the predicted proximity of the nucleotide and high-affinity calcium-binding sites of calreticulin (Fig. 2*B*). In line with these predictions, the absence of divalent cations (Ca^{2+} and Mg^{2+}) increased the K_m value for the ATPase activity of mCRT(WT) (K_m = 1.71 ± 0.05 mM). The presence of a single species of divalent cation also increased the K_m value for the ATPase activity of mCRT(WT) [K_m = 1.29 ± 0.01 mM (1 mM Mg^{2+} alone) and K_m = 1.41 ± 0.11 (5 mM Ca^{2+} only)] compared with the presence of both species (K_m = 0.47 ± 0.03 mM). Higher K_m values were observed for mCRT(K7A), mCRT(E8A), and mCRT(K63A) (Fig. 2*C* and Table 1). Consistent with the reduced abilities of these constructs to bind ATP, mCRT(D12A) and mCRT(R19A) were deficient in ATPase activity (Fig. 2*C* and Table 1), despite their abilities to bind nucleotides (Fig. 2*A* and Table 1), consistent with a model where Asp12 and Arg19 catalyze ATP hydrolysis. All of the mutants that affected ATP binding or hydrolysis migrated similar to mCRT(WT) by gel filtration chromatography (Fig. S2*A*) and were able to bind

Table 1. Nucleotide and calcium binding to calreticulin and ATP hydrolysis by calreticulin

Construct	Ligand	Technique	K_d, mM*	ΔH, kJ/mol*	Replicates	K_m, mM*	Replicates
mCRT(WT)	ATP	FQ	0.65 ± 0.09		30	0.47 ± 0.03	17
	ADP	FQ	1.02 ± 0.21		7		
	Ca^{2+}	ITC	0.017 ± 0.001	−89.50 ± 14.88	9		
mCRT(K7A)	ATP	FQ	6.33 ± 0.70		8	2.68 ± 0.07	17
	ADP	FQ	7.57 ± 1.56		3		
	Ca^{2+}	ITC	0.019 ± 0.004	−37.10 ± 9.63	4		
mCRT(E8A)	ATP	FQ	5.49 ± 1.45		5	2.51 ± 0.02	2
	ADP	FQ	8.52 ± 3.05		3		
	Ca^{2+}	ITC	ND†	ND†	3		
mCRT(D12A)	ATP	FQ	1.08 ± 0.17		4	2.20 ± 0.04	4
	ADP	FQ	1.22 ± 0.03		3		
	Ca^{2+}	ITC	0.02 ± 0.002	−18.64 ± 6.73	4		
mCRT(R19A)	ATP	FQ	1.03 ± 0.16		3	2.01 ± 0.25	3
	ADP	FQ	1.53 ± 0.14		3		
	Ca^{2+}	ITC	0.019 ± 0.005	−14.09 ± 5.12	4		
mCRT(K63A)	ATP	FQ	2.69 ± 0.58		2	2.04 ± 0.22	3
	ADP	FQ	1.69 ± 0.35		2		
	Ca^{2+}	ITC	0.018 ± 0.004	−28.35 ± 12.22	3		
mCRT(D311A)	ATP	FQ	2.45 ± 0.5		4	1.33 ± 0.23	4
	Ca^{2+}	ITC	ND†	ND†	2		
mCRT(Q50A)	ATP	FQ	1.18 ± 0.25		4	0.61 ± 0.08	3
mCRT(R145A)	ATP	FQ	0.52 ± 0.04		3	0.44 ± 0.08	2
mCRT(K305A)	ATP	FQ	0.52 ± 0.17		3	0.50 ± 0.08	2
mCRT(K334A)	ATP	FQ	0.78 ± 0.25		5	0.52 ± 0.11	3
mCRT(Y92A)	ATP	FQ	0.84 ± 0.09		2	0.45 ± 0.03	2

FQ, fluorescence quenching; ITC, isothermal titration calorimetry.
*Values represent mean ± SEM.
†No binding detected by the indicated method.

to the cochaperone ERp57 (Fig. S2*B*). Thus, the mutants are folded, nonaggregated, and functional for cochaperone binding. Together, these results are consistent with a model in which Lys7, Glu8, and Lys63 contribute to the stability of nucleotide binding and Asp12 and Arg19 are important for ATP hydrolysis (Fig. 2*B*). Residues that affected ATP binding or hydrolysis by mCRT are conserved in mammalian calreticulins (Fig. S3*A*). In some cases, calreticulins from other taxa, with greater sequence divergence from mammalian calreticulins (Fig. S3*B*), may have altered configurations of residues important for ATP binding, which needs further elucidation.

Calcium Binding Is Required for High-Affinity Nucleotide Binding and Nucleotides Destabilize High-Affinity Calcium Binding. The proposed ATP-binding site is in close proximity to the high-affinity calcium-binding site within the globular domain of calreticulin (Fig. 2*B*). Asp311 is a calcium-binding residue within the high-affinity calcium-binding site of calreticulin (14, 15, 19). mCRT(D311A) is impaired for high-affinity calcium binding, as assessed by isothermal titration calorimetry (ITC) assays (19) (Fig. 3*A* and Table 1). mCRT(D311A) also has a reduced affinity for ATP and a corresponding increase in its K_m value for ATPase activity relative to mCRT(WT), although the effects of the mCRT(D311A) mutation on ATP binding, hydrolysis, and ATP-induced thermostability changes were less significant than those effects measured with the key ATP site mutant mCRT(K7A) (Fig. 3 *B* and *C* and Table 1). Conversely, several mutants within the predicted ATP-binding site (Fig. 2*B*) [mCRT (K7A), mCRT(K63A), mCRT(D12A), and mCRT(R19A)] bound Ca^{2+} with affinities similar to the affinity for mCRT(WT) (Fig. 3*A* and Table 1), but with reduced binding enthalpies. Enthalpy-driven high-affinity calcium binding to mCRT(E8A) was essentially undetectable (Table 1), consistent with structural studies showing interactions of the peptide backbone of Glu8 with the Ca^{2+} ion in the high-affinity calcium-binding site (15). Furthermore, the presence of both ATP and ADP abrogated enthalpy-driven high-affinity calcium binding to mCRT(WT) (Fig. 3*A*). Together, these findings are consistent with the proposed model of distinct but proximal nucleotide and high-affinity calcium-binding sites (Fig. 2*B*), with Glu8 contributing to both sites. Nucleotides and mutants that affect nucleotide binding or hydrolysis influence enthalpy-driven calcium binding, and, conversely, a calcium-binding site mutant influences ATP binding and hydrolysis. Notably, distinct calcium- and ATP-binding phenotypes are observed for key mutants within each site (Fig. 3 and Table 1). mCRT(E8A) was not used for further functional studies due to the significant effects on both ATP and high-affinity calcium binding.

In Silico Predictions of ATP-Induced Destabilization of Synthetic Glycan Binding to Calreticulin. In chaperone systems, such as HSP70, nucleotide binding and hydrolysis alter the affinity of the chaperone toward substrates, thereby driving the chaperone cycle (reviewed in 35, 36). Previously, the synthetic glycan Glcα1–3Manα1–2Manα1–2Man (G1M3) has been used as a model substrate to study calreticulin–glycan interactions (15, 17, 37, 38). To understand the effects of nucleotide binding and hydrolysis on calreticulin–substrate interactions, we performed MD simulations of calreticulin in complex with the synthetic glycan G1M3 in the presence or absence of ATP and ADP. The calculated binding energy of calreticulin for G1M3 in the nucleotide-free state is −55.12 kcal/mol compared with −19.4 kcal/mol in the presence of ATP, corresponding to an overall 2.8-fold reduction in binding affinity. In contrast, the interaction is predicted to be more favorable in the presence of ADP (with a calculated binding energy of −35.4 kcal/mol).

To understand better the basis for ATP-mediated reduction in the glycan-binding affinity of calreticulin, we performed covariance analyses on MD trajectories of mCRT–G1M3 complexes in the presence or absence of nucleotides (ATP or ADP). Covariance analysis reports on the coupled motions between distant regions of proteins. Results of the covariance analyses show that the distant residues located at the ATP- and glycan-binding sites

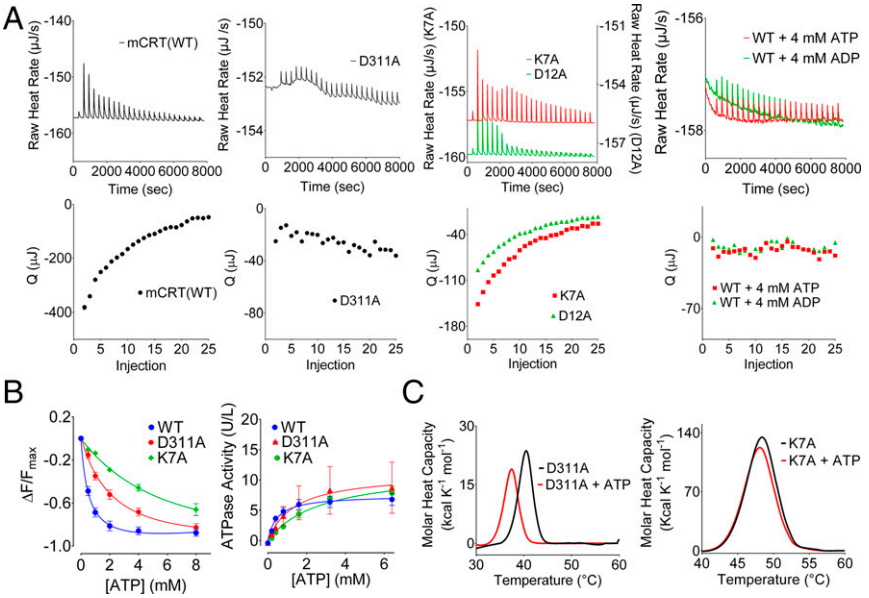

Fig. 3. Influences of nucleotides on calcium binding and of a calcium-binding site mutant on nucleotide binding. (*A*) Representative ITC thermograms depicting the binding of calcium to the high-affinity calcium-binding sites of the indicated calreticulin constructs in the absence or presence of 4 mM ATP or ADP. Plots show raw titration curves (*Upper*) and the corresponding curve fits (*Lower*). Data are representative of two to four [mCRT mutants: mCRT(WT) + ATP and mCRT(WT) + ADP] or nine [mCRT(WT)] independent experiments. Q, area of the indicated injection peak. (*B*, *Left*) Dose-dependent quenching of the Trp fluorescence of the indicated calreticulin constructs in the presence of varying concentrations of ATP. (*B*, *Right*) Michaelis–Menten kinetic plots and associated best global fit showing the rate of ATP hydrolysis by the indicated calreticulin constructs. Data show mean ± SEM. Binding and kinetic constants, along with data replicates, are shown in Table 1. ΔF, change in the intrinsic Trp fluorescence peak value relative to the ATP-free state; F_{max}, intrinsic Trp fluorescence peak value in the absence of ATP. (*C*) Representative DSC thermograms (of three to four independent experiments) showing ATP-induced thermostability changes for mCRT(D311A) (*Left*) and mCRT(K7A) (*Right*).

are coupled, exhibiting correlated motions (Fig. 4). Relative to the ATP-bound state, the correlated motions are reduced in the ADP-bound state and in the absence of nucleotide (Fig. 4, *Right* and *Left* vs. *Middle*). These findings suggest that dynamic coupling between the remote glycan- and nucleotide-binding sites of calreticulin following ATP binding could cause a reduction in glycan-binding affinity. As such, within the PLC, ATP binding could disfavor interactions between calreticulin and the glycan moiety of MHC class I, thereby destabilizing MHC class I–PLC interactions.

ATP Destabilizes Interactions Between Calreticulin and MHC Class I Molecules. To study how nucleotides influence interactions between calreticulin and MHC class I molecules, calreticulin-deficient MEFs (23) were labeled with [^{35}S]-methionine and the cell lysates were incubated with purified His-tagged mCRT(WT), mCRT (K7A), mCRT(D12A), mCRT(Y92A), or mCRT(D311A) immobilized on a nickel-agarose matrix. mCRT(Y92A) is a calreticulin mutant deficient in glycan binding (8, 17, 39), and the remaining mutants affect ATP binding, ATPase activity, or calcium and ATP binding as described above. The abilities of ATP or ADP to dissociate calreticulin-bound cellular proteins were compared. Relative to ADP, the presence of ATP enhanced protein recovery (Fig. 5*A*). These findings were further confirmed by comparing levels of ATP- and ADP-eluted total cellular proteins associated with the nickel-resin–immobilized calreticulin constructs by Coomassie staining of gels (Fig. 5*B*).

To assess glucosylation patterns of ATP eluates, MHC class I was immunoisolated from the [^{35}S]-methionine–labeled eluates of different calreticulin-bound beads, digested with endoglycosidase H_f (endoH; New England Biolabs) or Jack bean α-mannosidase (JBM; Sigma), and analyzed by SDS/PAGE (Fig. 5*C*, *Left*). JBM cleaves nine mannose residues from nonglucosylated N-linked glycans but only five residues from glucosylated glycans (40). EndoH catalyzes a more complete hydrolysis of glycans independent of their glucosylation state (41). Thus, the relative migration patterns of endoH and JBM digests can inform on protein glucosylation (17). All MHC class I samples recovered from the ATP eluates [except those samples eluted from mCRT(Y92A)] showed a slower migration in the JBM digest compared with the endoH digest, indicating glucosylation of the majority of the protein (Fig. 5*C*, *Left*). On the other hand, in the total imidazole eluate (in the absence of a cross-linker), only mCRT(K7A)-associated MHC I showed distinctly slower migration in the JBM digest compared with the endoH digest (Fig. 5*C*, *Middle*). Within imidazole-eluted samples, we have previously shown that the prior addition of a cross-linking agent can stabilize binding between calreticulin and glucosylated MHC class I (17). Consistent with those findings, in the presence of a cross-linker, all samples [except those samples eluted from mCRT(Y92A)] showed a slower migration of the JBM-digested protein compared with the endoH-digested sample (Fig. 5*C*, *Right*). Thus, both glucosylated and nonglucosylated MHC class I molecules associate with mCRT(WT), with a predominance of nonglucosylated MHC class I or glucosylated MHC class I, respectively, in the total imidazole eluates in the absence or presence of cross-linker (Fig. 5C, *Middle* and *Right*). Under all tested conditions, mCRT(Y92A) recruits nonglucosylated MHC class I (Fig. 5*C*), consistent with the known glycan-binding deficiency of this mutant (8, 17, 39). ATP induces the selective elution of monoglucosylated MHC class I from all calreticulin constructs capable of glycan binding (Fig. 5*C*, *Left*). Moreover, mCRT(K7A), which has the strongest impairment in ATP binding and ATPase activity (Fig. 2 and Table 1), is the only one of the tested calreticulin constructs that yields monoglucosylated MHC class I in the imidazole eluates in the absence of a cross-linker (Fig. 5*C*, *Middle*), indicating that mCRT(K7A) is able to maintain more stable binding to monoglucosylated MHC class I. Notably, this phenotype is not observable with mCRT(D311A), which has a primary calcium-binding impairment (Fig. 5*C*, *Middle*). mCRT (D311A) recruits monoglucosylated MHC class I similar to mCRT (WT) in the presence of a cross-linker (Fig. 5*C*, *Right*), indicating

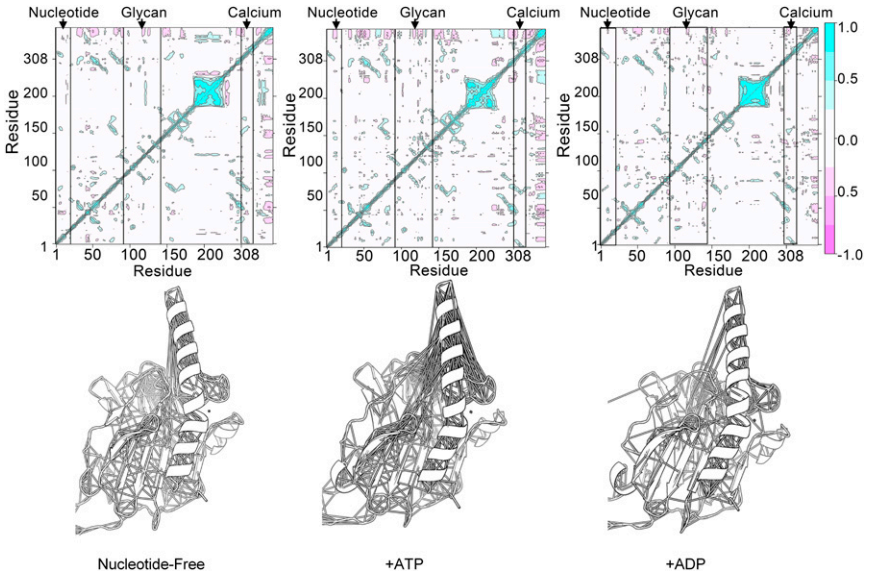

Fig. 4. ATP increases correlated residue motions in the globular domain of calreticulin. MD simulations were run of calreticulin in complex with G1M3 in the absence of nucleotides (*Left*) or in the presence of ATP (*Middle*) or ADP (*Right*). The figure shows the covariance matrices (*Upper*) and associated models of the globular domain of calreticulin with lines connecting the Cα atoms of residues whose motions were highly correlated ($|r| > 0.5$) over the course of the simulations (*Lower*). The covariance matrices are scaled from −1.0 (pink) to 1 (cyan). Cyan regions indicate that the Cα atoms move in a concerted way (positively correlated movements), and pink indicates opposite movements (anticorrelated motions). Levels are colored in increments of 0.25. Boxes denoted by arrows highlight residues surrounding the nucleotide (residues K7, E8, D12, and R19), glycan (residues Y92, K94, G107, D108, Y111, D118, and N137), and high-affinity calcium-binding (residue D311) sites in calreticulin. Correlated motions between the distant glycan- and ATP-binding regions are present in the ATP-bound state but are missing in the absence of nucleotides or in the presence of ADP. Note that the residue numbering is discontinuous from residue 228 onward to match the numbering in the X-ray structure [PDB ID code 3RG0 (16)] due to the P-domain truncation.

that high-affinity calcium binding, per se, is nonessential for calreticulin to bind monoglucosylated substrate.

Consistent with results from the total protein eluates (Fig. 5 *A* and *B*), MHC class I molecules were present in the ATP and total imidazole eluates of mCRT beads, but not in the ADP eluates (Fig. 5*D*, *Left*). Additionally, higher levels of MHC class I were recovered from ATP eluates of nickel-resin–immobilized mCRT (WT) compared with ATP eluates from mCRT(K7A), mCRT (D311A), and mCRT(Y92A) beads (Fig. 5*D*, *Right*). The lower yield of MHC class I in the mCRT(K7A) ATP eluates is consistent with impaired ATP binding and ATPase activity of mCRT(K7A) (Fig. 2 and Table 1). The lower yield of MHC class I in the mCRT (D311A) ATP eluates could relate to its partial impairment in ATP binding or ATPase activity (Fig. 3*B* and Table 1), as well as less effective ATP-transduced conformational changes. Compared with mCRT(WT), despite stronger overall MHC class I recruitment by mCRT(Y92A) (total imidazole elution in the absence of a cross-linker), ATP-induced MHC class I elution was less efficient (Fig. 5*D*). Because mCRT(Y92A) is not impaired in its ability to bind or hydrolyze ATP (Table 1) but is impaired for binding monoglucosylated forms of MHC class I (Fig. 5*C*), these findings suggest that ATP is more efficient at destabilizing glycan-mediated calreticulin–MHC class I interactions compared with glycan-independent interactions. Nonetheless, both glycan-dependent and glycan-independent calreticulin–MHC class I interactions are destabilized by ATP, because all of the tested calreticulin constructs yielded more total protein and MHC class I in the ATP eluates compared with the ADP eluates (Fig. 5 *A*, *B*, and *D*). It is also noteworthy that mCRT(Y92A) showed stronger or weaker MHC class I signals compared with mCRT(WT) in the total imidazole eluates without and with a cross-linker (Fig. 5*D*), which represent conditions for nonglucosylated and glucosylated MHC class I recruitment by mCRT(WT) (Fig. 5*C*, *Middle* and *Right*, respectively). These findings are consistent, respectively, with the stronger or impaired abilities of mCRT(Y92A) relative to mCRT(WT) to interact with polypeptide (8) and monoglucosylated substrates (17).

Mutations Affecting ATP or Calcium Binding Alter the Cellular Assembly of MHC Class I Molecules. To investigate the role of calreticulin–ATP interactions in regulating cellular calreticulin–MHC class I interactions and PLC dynamics, we expressed WT calreticulin and mutants deficient in ATP or high-affinity calcium binding in calreticulin-deficient MEFs (23). Mutants were expressed at comparable levels to mCRT(WT) in the total cell lysates (Fig. S4). Pulse–chase studies were conducted, followed by cell lysis in the presence of a reversible cross-linker, and sequential immunoprecipitations (IPs) with anti-calreticulin (first) and anti-MHC class I (second) were undertaken (Fig. 6*A*). From these analyses, no significant differences were found in the amounts of MHC class I recruited to the mutant calreticulin compared with mCRT(WT), except in the case of mCRT(Y92A), which showed delayed recruitment of the MHC class I. Notably, however, all of the mutants showed delayed rates of MHC class I dissociation from calreticulin, relative to mCRT(WT) (Fig. 6*A*).

Following the second IP of the sequential IPs, the MHC class I samples were also enzymatically digested with endoH (Fig. 6*B*, lanes 2 and 3) and JBM (Fig. 6*B*, lanes 4–14) to examine the glucosylation state of calreticulin-associated MHC class I. The endoH-digested MHC class I migrated more rapidly than JBM-digested MHC class I at all tested time points (Fig. 6*B*, lanes 2 and 3 compared with lanes 4 and 12), indicating that glucosylated MHC class I is associated with all of the calreticulins, including mCRT (Y92A). Digestions with glucosidase II (Glc) were further undertaken at different stages of the sequential IPs to assess whether the MHC class I-linked glucose moiety is, in fact, calreticulin-bound. Glc was added either after the first IP (anti-CRT), when calreticulin–MHC complexes were still maintained via the cross-linker, or after the second IP (anti-MHC class I IP), when calreticulin–MHC class I complexes had been dissociated via the use of a reducing agent to reverse the cross-linking. With mCRT(WT), mCRT(K7A),

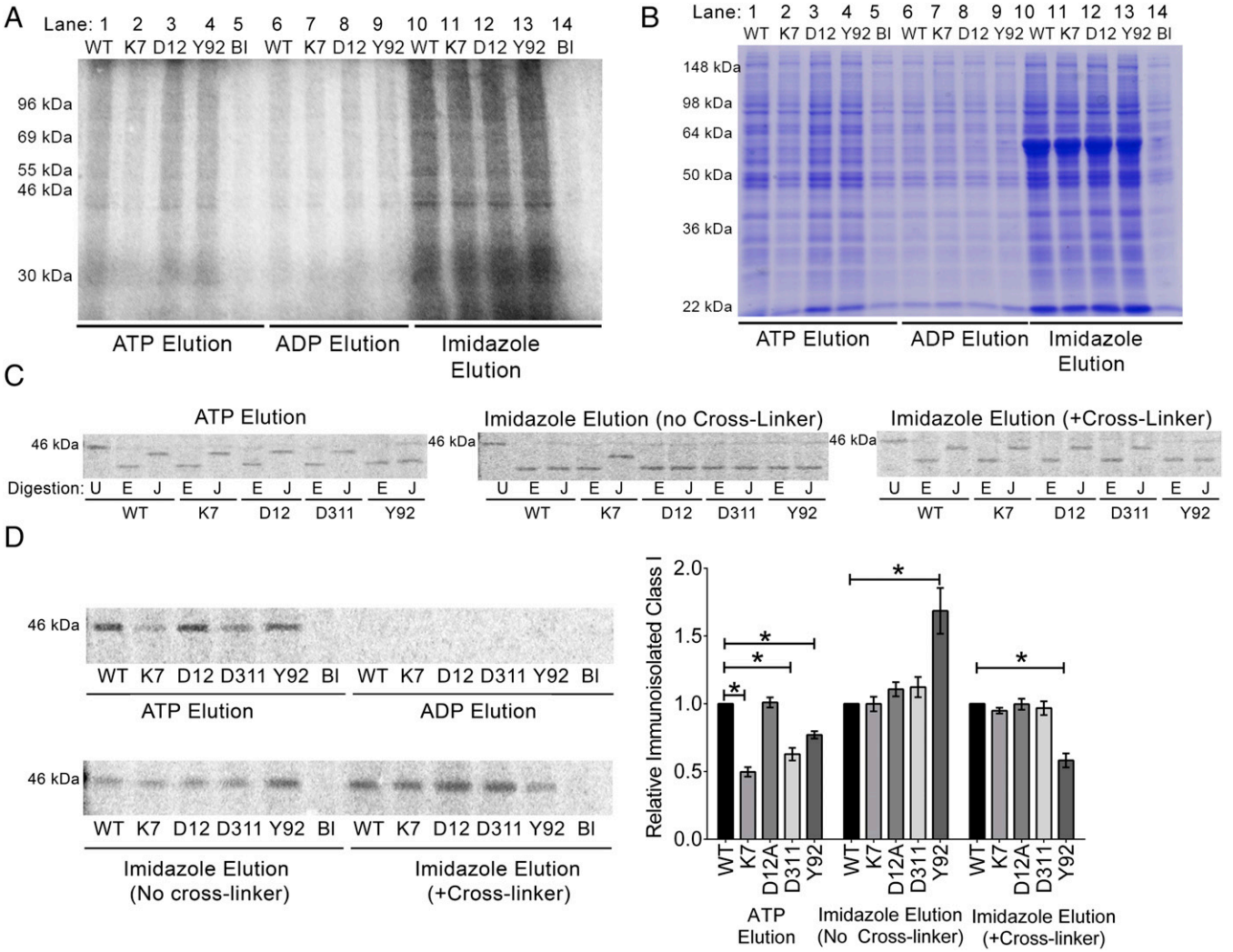

Fig. 5. ATP destabilizes the interaction of calreticulin with cellular substrates. Lysates from calreticulin-deficient MEFs that were [^{35}S]-methionine–labeled (*A*, *C*, and *D*) or unlabeled (*B*) were incubated with the indicated nickel-resin–immobilized calreticulin [WT = mCRT(WT), K7 = mCRT(K7A), D12 = mCRT(D12A), D311 = mCRT(D311A), and Y92 = mCRT(Y92A)] or nickel-resin alone (BI). Following washes, protein elutions were performed with ATP, ADP, or imidazole as indicated. Total protein eluates were analyzed by SDS/PAGE and phosphorimaging (*A*) or Coomassie staining (*B*). MHC class I was further immunoprecipitated from the indicated bead eluates, enzymatically digested (*C*) or directly quantified (*D*), and visualized by SDS/PAGE and phosphorimaging. (*C*) EndoH digests are labeled E, JBM digests are labeled J, and undigested protein is labeled U. (*Right*) Lysates were bound to beads in the presence of the reversible cross-linker dimethyl 3,3′-dithiobispropionimidate before washing beads and elution with imidazole. Data are representative of five ATP vs. ADP eluate comparisons (*A*), three ATP vs. ADP eluate comparisons (*B*), two to four (D311A ATP and imidazole elutions) or seven to 12 (other constructs) (*C*), and five to six (D311A and D12A) or 10–17 (other constructs) (*D*) independent analyses. (*D*, *Right*) Quantification of the levels of immunoisolated MHC class I, averaged from all replicates [each normalized to the corresponding mCRT(WT) signals]. Data show mean ± SEM, with statistical significance assessed via a two-way ANOVA followed by a Dunnett's post hoc test. Statistically significant means are indicated (*).

mCRT(D12A), and mCRT(D311A), when Glc was added following the first IP (but was absent during the JBM digestion step, which was done following the second IP), the JBM digestion patterns were unaltered and endoH/JBM migration differences persisted (Fig. 6*B*, lanes 4, 6, 9, and 12 compared with lanes 5, 7, 10, and 13). A distinct Glc digestion pattern was seen with mCRT(Y92A), where digestion with Glc after the first IP resulted in the generation of a lower molecular-weight JBM product (Fig. 6*B*, lanes 4, 6, 9, and 12 compared with lanes 5, 7, 10, and 13). When Glc was added after the second IP (same step as the JBM digest, after cross-linking is reversed), the presence of Glc in all cases yielded smaller molecular-weight products compared with JBM alone and the endoH/JBM migration differences were lost (Fig. 6*B*, lanes 6, 9, and 12 compared with lanes 8, 11, and 14). These findings suggest that when in complex with mCRT(WT), mCRT(K7A), mCRT(D12A), and mCRT(D311A), the glucose moiety of MHC class I is inaccessible following the first IP (via calreticulin engagement). On the other hand, consistent with the inability of mCRT(Y92A) to bind glycans (8, 17), the glucose moiety of associated MHC class I is accessible to Glc following the first IP, indicating important differences in the modes of MHC class I recruitment by mCRT (Y92A) compared with all other mCRT constructs. Notably, the absence of high-affinity calcium binding in the mCRT(D311A) mutant did not significantly affect the efficiency of glucosylated MHC class I recruitment to calreticulin.

In the ER, calreticulin facilitates formation of the PLC (reviewed in 2) and retrieves suboptimally assembled MHC class I from post-ER compartments (42). Prolonged calreticulin binding of MHC class I in the context of mCRT(K7A), mCRT(D12A), and mCRT(D311A) translated to prolonged TAP binding (Fig. 6*C*). Additionally, the overall rate of trafficking of MHC class I from the ER was retarded for mCRT(K7A), mCRT(D12A), and mCRT (D311A) compared with mCRT(WT), resulting in prolonged endoH sensitivity as assessed by direct anti-MHC class I IPs and enzymatic

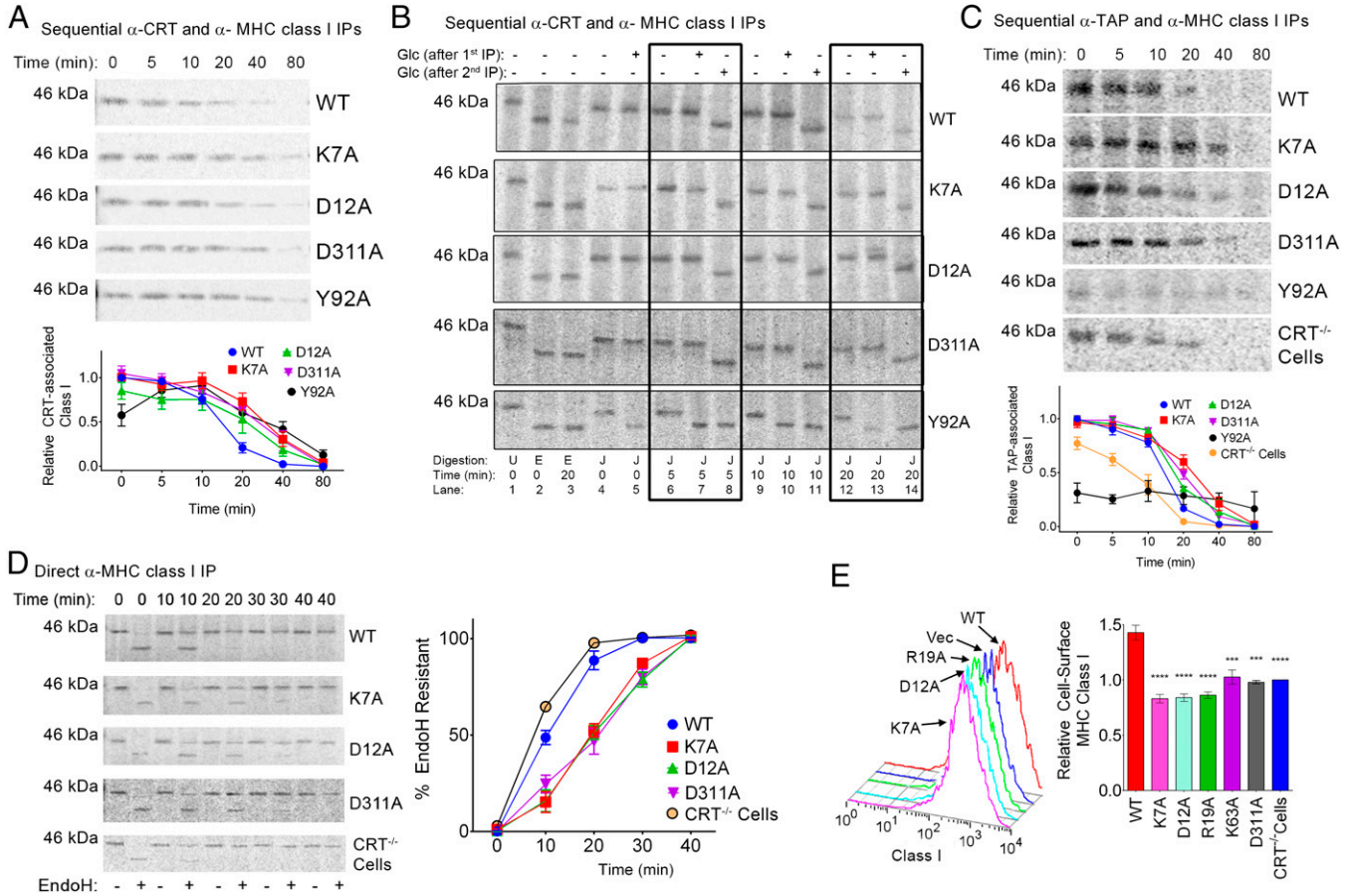

Fig. 6. Delayed maturation kinetics and suboptimal assembly of MHC class I molecules in cells expressing calreticulin mutants that disrupt ATP or high-affinity calcium binding: CRT$^{-/-}$ MEFs were infected with retroviruses encoding the indicated calreticulin constructs and further analyzed for MHC class I interactions with calreticulin (*A* and *B*) or TAP (*C*), or for their rates of maturation (*D*) and cell surface expression (*E*). (*A–D*) MEFs expressing the indicated calreticulin constructs were [^{35}S]-methionine–labeled and chased for the indicated times, and proteins in lysates were immunoprecipitated as indicated. Recovered proteins were visualized by SDS/PAGE and phosphorimaging analyses. (*A* and *B*) Sequential anti-calreticulin (first IP) and anti-MHC class I (second IP) IPs were performed on cell lysates. (*A*) mCRT-associated MHC class I levels were quantified at the indicated time points. (*B*) Immunoprecipitated proteins were digested with J or E following the second IP. Additionally, Glc was present after the first or second IP as indicated. Boxes highlight the 5- and 20-min time points of the chase. (*C*) Sequential anti-TAP (first IP) and anti-MHC class I (second IP) IPs were performed on cell lysates, and TAP-associated MHC class I levels were assessed. (*D*) Direct anti-MHC class I IPs were performed, and the immunoisolated protein was digested with endoH. Graphs show data averaged across four to nine (*A*), two to five (*C*), and three to four (*D*) independent analyses from two to four independent infections. All signals were normalized relative to the mCRT(WT) signal at the zero time point analyzed within the same experiment. (*E*) Flow cytometric analyses of cell surface MHC class I expression. (*Left*) Representative histograms depicting the cell-surface MHC class I levels in MEFs expressing the indicated calreticulin constructs or lacking calreticulin expression (Vec). (*Right*) Mean cell surface MHC class I levels ± SEM normalized to cells lacking calreticulin expression (Vec or CRT$^{-/-}$ cells). Data represent the average of four to seven [mCRT(D311A), mCRT(D12A), mCRT(R19A), and mCRT(K63A)], 15 [mCRT(K7A)], or 22 [mCRT(WT) and CRT$^{-/-}$ cells] independent experiments. Statistical significance was assessed via a one-way ANOVA followed by a Dunnett's post hoc test, with statistically significant means [relative to mCRT(WT)] denoted (*).

digestions (Fig. 6*D*). Consistent with previous reports (8), MHC class I is recruited to TAP less efficiently in the content of mCRT(Y92A) compared with mCRT(WT) (Fig. 6*C*). On the other hand, there were no significant differences in the amount of MHC class I recruited to TAP in the context of mCRT(K7A), mCRT(D12A), and mCRT9(D311A), although all three mutations resulted in slower MHC class I dissociation from TAP (Fig. 6*C*). Also consistent with previous findings (5, 8, 37) is the observation that MHC class I recruitment to TAP is less efficient and less stable in calreticulin-deficient cells compared with their mCRT(WT)-reconstituted counterparts (Fig. 6*C*), and that the overall rate of MHC class I endoH resistance acquisition is accelerated under conditions of calreticulin deficiency (Fig. 6*D*).

The MHC class I maturation differences in cells expressing calreticulin mutants that affect ATP binding or hydrolysis translated into reduced cell-surface expression of MHC class I. Previously, calreticulin mutants deficient in glycan and ERp57 binding were found to be unable to restore surface MHC class I levels to the same extent as mCRT(WT) (5, 8). Likewise, MEFs expressing mCRT (WT) had higher levels of surface MHC class I relative to MEFs lacking calreticulin or MEFs expressing calreticulin constructs deficient in nucleotide binding [mCRT(K7A) and mCRT(K63A)] or hydrolysis [mCRT(D12A) and mCRT(R19A)] ($P < 0.05$) (Fig. 6*E*). Cells expressing mCRT(D311A) also displayed significantly reduced levels of cell-surface MHC class I ($P < 0.05$) (Fig. 6*E*). Together, these findings suggest that ATP binding and calcium binding by calreticulin are key elements governing PLC dynamics and the maturation of cellular MHC class I molecules.

Discussion

This study highlights roles for calreticulin–ATP and calreticulin–calcium interactions in regulating PLC dynamics. Thus far, attempts to define the nucleotide-binding site of mCRT via X-ray crystallography have not been successful (15). Based on our findings, it is likely that cocrystallization of the mCRT–ATP complex is hindered by ATP-induced conformational changes within the

globular domain of calreticulin that impede its ability to form an ordered crystal lattice. In the absence of a crystal structure of a calreticulin–nucleotide complex, the computational and experimental approaches described in this study allowed for the identification of calreticulin mutants that are impaired in ATP binding and hydrolysis, and for an ATP interaction site to be modeled (Figs. 1 and 2). Although, a number of our studies point to direct interactions of residues, such as mCRT(K7A) and mCRT(D12A), with nucleotide (Figs. 1–3 and Movies S1 and S2), it remains possible that ATP binding and/or ATPase impairments of these mutants result from more indirect contributions. Regardless of the precise mechanism, the functional impairments of the selected mutants in ATP binding and/or hydrolysis (Figs. 1 and 2) validate their further use as tools to understand better the effects of calreticulin–ATP interactions upon substrate binding and release (Figs. 5 and 6).

ATP binding reduces the thermostability of calreticulin (Fig. 1), disrupts enthalpy-driven high-affinity calcium binding (Fig. 3), increases molecular motions within the globular domain of calreticulin (as seen in MD simulations) (Fig. 4), and promotes dissociation of calreticulin–substrate complexes (Figs. 5 and 6). Within the PLC, these ATP-induced structural changes could comprise the mechanism by which ATP binding facilitates the release of MHC class I from calreticulin, resulting in its exit from the PLC (Fig. 7). It is noteworthy that although both ATP and ADP disrupt enthalpy-driven calcium binding by calreticulin (Fig. 3), only ATP induces the dissociation of cellular MHC class I (Fig. 5). Additionally, impaired ATP binding delays dissociation of glucosylated MHC class I from calreticulin (Figs. 5*C* and 6 *A* and *B*). Previous findings have shown that zinc can interact with calreticulin and induce marked conformational changes (11, 12, 43). Further studies are needed to understand the effects of ATP on zinc binding by calreticulin and whether ATP and zinc might synergize to affect substrate dissociation.

In all anti-calreticulin IPs [with the exception of mCRT(Y92A)], glucosylated forms of MHC class I were bound to calreticulin (Fig. 6*B*). ATP has been shown to induce the in vitro polypeptide-specific chaperone activity of calreticulin, particularly at elevated temperatures and in the context of mCRT(ΔP) (8, 12). However, within the MHC class I assembly pathway, no differences in glycan-dependent vs. glycan-independent binding modes were noted for mCRT(WT) and ATP- or calcium-binding site mutants (Fig. 6*B*). On the other hand, mCRT(Y92A) showed a distinct lack of glycan engagement (Fig. 6*B*). Thus, within the PLC, a calreticulin mutant impaired for glycan binding can engage MHC class I via glycan-independent interactions, but interactions with glucosylated MHC class I predominate in the context of mCRT(WT), as well as ATP- and calcium-binding–deficient mutants.

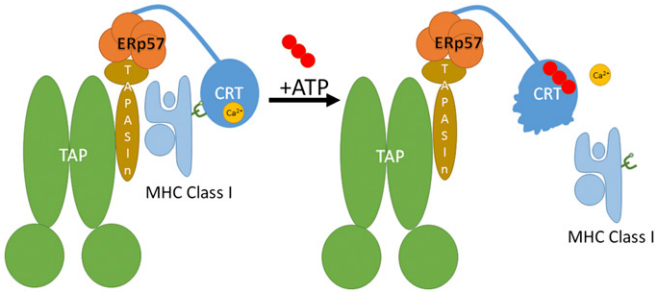

Fig. 7. Proposed role for ATP in promoting the release of MHC class I from the PLC. Within the PLC, calreticulin functions as a chaperone to stabilize MHC class I interactions with the PLC. Interaction of calreticulin with ATP is predicted to destabilize the globular domain of calreticulin, thereby releasing the folded MHC class I in addition to dissociating the high-affinity calcium ion from the globular domain of calreticulin. Whether ATP is hydrolyzed during this step needs further assessment.

Previous studies have shown that calcium binding stabilizes the globular domain of calreticulin (11, 19, 43). Here, we show that mCRT(D311A), which is impaired in high-affinity calcium binding, has a reduced affinity for ATP and a reduced ATPase activity (Fig. 3 and Table 1), likely due to the reduced basal structural rigidity of mCRT(D311A) (Figs. 1*E* and 3*C*), which hinders ATP binding. In turn, the extent of ATP-induced conformational changes is affected, which prolongs interactions between calreticulin and cellular substrates, such as MHC class I (Fig. 6).

mCRT(D12A) reduces ATP binding by ∼1.7-fold and ATPase activity by fivefold (Fig. 2 and Table 1). However, ATP promotes elution of glucosylated MHC class I from matrix-immobilized mCRT(D12A) to a similar extent as mCRT(WT) (Fig. 5*C*), suggesting that ATPase activity, per se, is nonessential for inducing MHC class I dissociation. On the other hand, mCRT(K7A) and mCRT(D311A), which have stronger impairments in ATP binding compared with mCRT(D12A) (Table 1), were less effective than mCRT(WT) for ATP-induced elution of MHC class I (Fig. 5*C*). Although these findings suggest that ATP binding alone (rather than ATP binding and hydrolysis) drives MHC class I dissociation, it is noteworthy that mCRT(D12A) has similar effects as mCRT(K7A) and mCRT(D311A) in reducing the rate of MHC class I dissociation from calreticulin and TAP (Fig. 6). ERp57 (which represents the first point of calreticulin interaction with the PLC; Fig. 7), per se, does not affect the ATPase activity of calreticulin (K_m = 0.57 ± 0.07 mM). Additional studies are needed to understand better whether MHC class I molecules, which represent a second point of calreticulin interaction with the PLC (Fig. 7), influence the ATPase activity of calreticulin, which will require sufficient quantities of purified glucosylated MHC class I for further biochemical assessments. Moreover, similar to the BiP chaperone cycle (reviewed in 44), there may be a more complex involvement of nucleotide exchange and ATPase activating factors that accounts for similar cellular phenotypes of the mCRT(K7A) and mCRT(D12A) mutants.

In conclusion, this study shows that ATP binding influences the interactions of calreticulin with cellular substrates, and that ATP and calcium binding to calreticulin influences the stability of the PLC. Further studies are needed to understand better the potential synergy between ATP and peptides in driving MHC class I dissociation. In addition to its role in the PLC, a large number of cell-surface and secreted glycoproteins are substrates for calreticulin. The results of this investigation thus have broad significance toward understanding the cellular mechanisms of protein quality control.

Materials and Methods

Calreticulin Expression. Methods for expression and purification of mCRT constructs are described in *SI Materials and Methods* and based on published procedures (8, 19). Other methods, including DSC, ITC, and flow cytometry, are also based on previously published procedures (8, 19) and are briefly described in *SI Materials and Methods*.

Molecular Modeling. Docking of ATP to calreticulin and associated MD simulations are described in *SI Materials and Methods*.

Fluorescence Quenching. Steady-state affinities of calreticulin toward ATP and ADP were measured as described earlier (16). Calreticulin [at a concentration of 0.5 mg/mL in 20 mM Hepes (pH 7.5), 10 mM NaCl, and 5 mM $CaCl_2$] was incubated with 0–8 mM ATP or ADP, and the Trp fluorescence of the protein was measured from 310–390 nm following excitation at 280 nm. All measurements were made at 21 °C using a Fluoromax-3 spectrophotometer (Horiba Scientific) or a SpectraMax M5 plate reader (Molecular Devices). Changes in Trp fluorescence peak intensities at each nucleotide concentration were normalized relative to the peak intensity in the absence of nucleotide and plotted as a function of nucleotide concentration. The steady-state affinity of calreticulin toward nucleotides was calculated via nonlinear least squares regression using a one site-specific model in GraphPad Prism.

ATPase Assay. ATPase measurements were performed using a QuantiChrom ATPase/GTPase assay kit (BioAssay Systems). Calreticulin (0.2 μM) was incubated with varying [ATP] in 20 mM Hepes (pH 7.5), 10 mM NaCl, 5 mM

$CaCl_2$, and 1 mM $MgCl_2$ for 15 min at 37 °C in a 96-well microplate (total reaction volume of 40 μL). The reaction was stopped, and the chromophore was developed via the addition of 200 μL of malachite green reagent and incubation at room temperature for 30 min. Absorbance measurements were undertaken at 620 nm using a BIO-TEK spectrophotometer. Measurement of the ATPase rate of mCRT(WT) in the absence of Ca^{2+} and/or Mg^{2+} was undertaken via the addition of 5 mM EDTA to mCRT(WT), followed by three rounds of dialysis in 20 mM Hepes (pH 7.5) and 10 mM NaCl to ensure complete removal of residual divalent cations and EDTA. $CaCl_2$ (5 mM) and/or $MgCl_2$ (1 mM) was added back to mCRT(WT) as needed before incubation with ATP. For all analyses, the ATPase rates were plotted against ATP concentration and analyzed in GraphPad Prism via nonlinear least squares regression.

Metabolic Labeling, Calreticulin Binding, and IP Analyses. Binding of [^{35}S]-methionine–pulsed cell lysates to nickel-nitrilotriacetic acid–immobilized calreticulin in the absence of a cross-linker was undertaken as described previously (17) and is briefly described in *SI Materials and Methods*. In indicated analyses, cross-linker was present during the lysate-calreticulin bead incubation step. All ATP/ADP elutions were performed following calreticulin-cell lysate binding in the absence of a cross-linker. Procedures for sequential (anti-TAP or anti-calreticulin) or direct MHC class I immunoisolation are described in *SI Materials and Methods*.

ACKNOWLEDGMENTS. We thank Dr. Jason Getswicki and Dr. Mi Lim for use of the spectrofluorometer. We also thank Maria Wooten for early contributions to the project, Dr. Syed Monem Rizvi for assistance with pulse–chase studies, and Dr. Nicole Koropatkin for helpful discussions relating to ITC data analyses. This work used the DNA Sequencing and Hybridoma Cores of the University of Michigan. The research reported in this publication was supported by National Institute of Allergy and Infectious Diseases of the National Institutes of Health (NIAID/NIH) Award R01AI066131 (to M.R.), by a University of Michigan Bridge award, and by the University of Michigan Fast Forward Protein Folding Diseases Initiative. Additional financial support was obtained from American Heart Association Postdoctoral Fellowship 12POST8810006 (to S.J.W.) and from NIAID/NIH Award R01AI044115 (to M.R.).

1. Blum JS, Wearsch PA, Cresswell P (2013) Pathways of antigen processing. *Annu Rev Immunol* 31:443–473.
2. Raghavan M, Wijeyesakere SJ, Peters LR, Del Cid N (2013) Calreticulin in the immune system: Ins and outs. *Trends Immunol* 34(1):13–21.
3. Rizvi SM, Del Cid N, Lybarger L, Raghavan M (2011) Distinct functions for the glycans of tapasin and heavy chains in the assembly of MHC class I molecules. *J Immunol* 186(4):2309–2320.
4. Wearsch PA, Peaper DR, Cresswell P (2011) Essential glycan-dependent interactions optimize MHC class I peptide loading. *Proc Natl Acad Sci USA* 108(12):4950–4955.
5. Gao B, et al. (2002) Assembly and antigen-presenting function of MHC class I molecules in cells lacking the ER chaperone calreticulin. *Immunity* 16(1):99–109.
6. Garbi N, Tanaka S, Momburg F, Hämmerling GJ (2006) Impaired assembly of the major histocompatibility complex class I peptide-loading complex in mice deficient in the oxidoreductase ERp57. *Nat Immunol* 7(1):93–102.
7. Zhang Y, Baig E, Williams DB (2006) Functions of ERp57 in the folding and assembly of major histocompatibility complex class I molecules. *J Biol Chem* 281(21):14622–14631.
8. Del Cid N, et al. (2010) Modes of calreticulin recruitment to the major histocompatibility complex class I assembly pathway. *J Biol Chem* 285(7):4520–4535.
9. Rizvi SM, Raghavan M (2006) Direct peptide-regulatable interactions between MHC class I molecules and tapasin. *Proc Natl Acad Sci USA* 103(48):18220–18225.
10. Wearsch PA, Cresswell P (2007) Selective loading of high-affinity peptides onto major histocompatibility complex class I molecules by the tapasin-ERp57 heterodimer. *Nat Immunol* 8(8):873–881.
11. Corbett EF, et al. (2000) The conformation of calreticulin is influenced by the endoplasmic reticulum luminal environment. *J Biol Chem* 275(35):27177–27185.
12. Saito Y, Ihara Y, Leach MR, Cohen-Doyle MF, Williams DB (1999) Calreticulin functions in vitro as a molecular chaperone for both glycosylated and non-glycosylated proteins. *EMBO J* 18(23):6718–6729.
13. Gribble FM, et al. (2000) A novel method for measurement of submembrane ATP concentration. *J Biol Chem* 275(39):30046–30049.
14. Chouquet A, et al. (2011) X-ray structure of the human calreticulin globular domain reveals a peptide-binding area and suggests a multi-molecular mechanism. *PLoS One* 6(3):e17886.
15. Kozlov G, et al. (2010) Structural basis of carbohydrate recognition by calreticulin. *J Biol Chem* 285(49):38612–38620.
16. Pocanschi CL, et al. (2011) Structural and functional relationships between the lectin and arm domains of calreticulin. *J Biol Chem* 286(31):27266–27277.
17. Wijeyesakere SJ, Rizvi SM, Raghavan M (2013) Glycan-dependent and -independent interactions contribute to cellular substrate recruitment by calreticulin. *J Biol Chem* 288(49):35104–35116.
18. Baksh S, Michalak M (1991) Expression of calreticulin in Escherichia coli and identification of its Ca2+ binding domains. *J Biol Chem* 266(32):21458–21465.
19. Wijeyesakere SJ, Gafni AA, Raghavan M (2011) Calreticulin is a thermostable protein with distinct structural responses to different divalent cation environments. *J Biol Chem* 286(11):8771–8785.
20. Frickel EM, et al. (2002) TROSY-NMR reveals interaction between ERp57 and the tip of the calreticulin P-domain. *Proc Natl Acad Sci USA* 99(4):1954–1959.
21. Ellgaard L, Frickel EM (2003) Calnexin, calreticulin, and ERp57: Teammates in glycoprotein folding. *Cell Biochem Biophys* 39(3):223–247.
22. Kozlov G, et al. (2010) Structural basis of cyclophilin B binding by the calnexin/calreticulin P-domain. *J Biol Chem* 285(46):35551–35557.
23. Nakamura K, et al. (2001) Functional specialization of calreticulin domains. *J Cell Biol* 154(5):961–972.
24. Wu G, Robertson DH, Brooks CL, 3rd, Vieth M (2003) Detailed analysis of grid-based molecular docking: A case study of CDOCKER-A CHARMm-based MD docking algorithm. *J Comput Chem* 24(13):1549–1562.
25. Brooks BR, et al. (2009) CHARMM: The biomolecular simulation program. *J Comput Chem* 30(10):1545–1614.
26. Morris GM, et al. (2009) AutoDock4 and AutoDockTools4: Automated docking with selective receptor flexibility. *J Comput Chem* 30(16):2785–2791.
27. Lee MS, Salsbury FR, Brooks CL (2002) Novel generalized Born methods. *J Chem Phys* 116(24):10606–10614.
28. Lee MS, Feig M, Salsbury FR, Jr, Brooks CL, 3rd (2003) New analytic approximation to the standard molecular volume definition and its application to generalized Born calculations. *J Comput Chem* 24(11):1348–1356.
29. Prodromou C, et al. (1997) Identification and structural characterization of the ATP/ADP-binding site in the Hsp90 molecular chaperone. *Cell* 90(1):65–75.
30. Vieth M, Hirst JD, Dominy BN, Daigler H, Brooks CL (1998) Assessing search strategies for flexible docking. *J Comput Chem* 19(14):1623–1631.
31. Barril X, et al. (2005) Structure-based discovery of a new class of Hsp90 inhibitors. *Bioorg Med Chem Lett* 15(23):5187–5191.
32. Shoichet BK, Kobilka BK (2012) Structure-based drug screening for G-protein-coupled receptors. *Trends Pharmacol Sci* 33(5):268–272.
33. Aravind L, Koonin EV (1999) DNA polymerase beta-like nucleotidyltransferase superfamily: Identification of three new families, classification and evolutionary history. *Nucleic Acids Res* 27(7):1609–1618.
34. Nadeau K, Das A, Walsh CT (1993) Hsp90 chaperonins possess ATPase activity and bind heat shock transcription factors and peptidyl prolyl isomerases. *J Biol Chem* 268(2):1479–1487.
35. Mayer MP (2010) Gymnastics of molecular chaperones. *Mol Cell* 39(3):321–331.
36. Stirling PC, Bakhoum SF, Feigl AB, Leroux MR (2006) Convergent evolution of clamp-like binding sites in diverse chaperones. *Nat Struct Mol Biol* 13(10):865–870.
37. Jeffery E, Peters LR, Raghavan M (2011) The polypeptide binding conformation of calreticulin facilitates its cell-surface expression under conditions of endoplasmic reticulum stress. *J Biol Chem* 286(4):2402–2415.
38. Kapoor M, et al. (2003) Interactions of substrate with calreticulin, an endoplasmic reticulum chaperone. *J Biol Chem* 278(8):6194–6200.
39. Kapoor M, et al. (2004) Mutational analysis provides molecular insight into the carbohydrate-binding region of calreticulin: Pivotal roles of tyrosine-109 and aspartate-135 in carbohydrate recognition. *Biochemistry* 43(1):97–106.
40. Cannon KS, Helenius A (1999) Trimming and readdition of glucose to N-linked oligosaccharides determines calnexin association of a substrate glycoprotein in living cells. *J Biol Chem* 274(11):7537–7544.
41. Tarentino AL, Plummer TH, Jr, Maley F (1974) The release of intact oligosaccharides from specific glycoproteins by endo-beta-N-acetylglucosaminidase H. *J Biol Chem* 249(3):818–824.
42. Howe C, et al. (2009) Calreticulin-dependent recycling in the early secretory pathway mediates optimal peptide loading of MHC class I molecules. *EMBO J* 28(23):3730–3744.
43. Li Z, Stafford WF, Bouvier M (2001) The metal ion binding properties of calreticulin modulate its conformational flexibility and thermal stability. *Biochemistry* 40(37):11193–11201.
44. Behnke J, Feige MJ, Hendershot LM (2015) BiP and its nucleotide exchange factors Grp170 and Sil1: Mechanisms of action and biological functions. *J Mol Biol* 427(7):1589–1608.
45. Ellgaard L, et al. (2001) NMR structure of the calreticulin P-domain. *Proc Natl Acad Sci USA* 98(6):3133–3138.
46. Yang J, et al. (2015) The I-TASSER Suite: Protein structure and function prediction. *Nat Methods* 12(1):7–8.
47. Trott O, Olson AJ (2010) AutoDock Vina: Improving the speed and accuracy of docking with a new scoring function, efficient optimization, and multithreading. *J Comput Chem* 31(2):455–461.
48. Kollman PA, et al. (2000) Calculating structures and free energies of complex molecules: Combining molecular mechanics and continuum models. *Acc Chem Res* 33(12):889–897.
49. Hämmerling GJ, Rüsch E, Tada N, Kimura S, Hämmerling U (1982) Localization of allodeterminants on H-2Kb antigens determined with monoclonal antibodies and H-2 mutant mice. *Proc Natl Acad Sci USA* 79(15):4737–4741.
50. Schneider CA, Rasband WS, Eliceiri KW (2012) NIH Image to ImageJ: 25 years of image analysis. *Nat Methods* 9(7):671–675.
51. Persson S, et al. (2003) Phylogenetic analyses and expression studies reveal two distinct groups of calreticulin isoforms in higher plants. *Plant Physiol* 133(3):1385–1396.